the plant journal

SEB SOCIETY FOR EXPERIMENTAL BIOLOGY

The Plant Journal (2024) doi: 10.1111/tpj.16935

Strong heterologous electron sink outcompetes alternative electron transport pathways in photosynthesis

Michal Hubáček[1], Laura T. Wey[1], Robert Kourist[2], Lenny Malihan-Yap[2], Lauri Nikkanen[1] and Yagut Allahverdiyeva[1,*]

[1]*Molecular Plant Biology, Department of Life Technologies, University of Turku, Turku 20014, Finland, and*
[2]*Institute of Molecular Biotechnology, NAWI Graz, BioTechMed, Graz University of Technology, Graz 8010, Austria*

Received 26 February 2024; revised 27 May 2024; accepted 3 July 2024.
*For correspondence (e-mail allahve@utu.fi).

SUMMARY

Improvement of photosynthesis requires a thorough understanding of electron partitioning under both natural and strong electron sink conditions. We applied a wide array of state-of-the-art biophysical and biochemical techniques to thoroughly investigate the fate of photosynthetic electrons in the engineered cyanobacterium *Synechocystis* sp. PCC 6803, a blueprint for photosynthetic biotechnology, expressing the heterologous gene for ene-reductase, YqjM. This recombinant enzyme catalyses the reduction of an exogenously added substrate into the desired product by utilising photosynthetically produced NAD(P)H, enabling whole-cell biotransformation. Through coupling the biotransformation reaction with biophysical measurements, we demonstrated that the strong artificial electron sink, outcompetes the natural electron valves, the flavodiiron protein-driven Mehler-like reaction and cyclic electron transport. These results show that ferredoxin-NAD(P)H-oxidoreductase is the preferred route for delivering photosynthetic electrons from reduced ferredoxin and the cellular NADPH/NADP+ ratio as a key factor in orchestrating photosynthetic electron flux. These insights are crucial for understanding molecular mechanisms of photosynthetic electron transport and harnessing photosynthesis for sustainable bioproduction by engineering the cellular source/-sink balance. Furthermore, we conclude that identifying the bioenergetic bottleneck of a heterologous electron sink is a crucial prerequisite for targeted engineering of photosynthetic biotransformation platforms.

Keywords: photosynthesis, biotransformation, cyanobacteria, *Synechocsytis* sp. PCC6803, fluorescence, gas exchange.

INTRODUCTION

Oxygenic photosynthesis is driven by the photo-oxidation of water, liberating electrons which are eventually used to produce the photosynthetic reductant NADPH for carbon fixation and metabolism (Figure 1a) (Hitchcock et al., 2022; Mullineaux, 2014; Nikkanen et al., 2021). The soluble electron carrier protein ferredoxin (Fd) is the electron distribution hub of photosynthesis (Figure 1b) (Goss & Hanke, 2014; Hanke & Mulo, 2013; Nikkanen et al., 2021). However, the factors determining the fate of electrons from Fd remain poorly understood. Elucidating this is imperative towards understanding how photosynthetic organisms balance their light reactions with carbon fixation and downstream cell metabolism in response to changing environmental conditions and to rationally harness photosynthetic microorganisms as green cell factories for sustainable bioproduction (Allahverdiyeva et al., 2021; Barbosa et al., 2023; Hitchcock et al., 2022; Santos-Merino et al., 2023; Tan et al., 2022).

Reduced Fd (Fd_{red}) is predominantly oxidised by ferredoxin-$NADP^+$-oxidoreductase (FNR) to produce NADPH in the final step of LET. The generated trans-thylakoidal proton motive force (*pmf*), composed of proton and electrical gradients, is utilised by the ATP synthase to produce ATP. Both NADPH and ATP fuel the CBB cycle and various downstream metabolic processes. However, the LET alone does not generate sufficient ATP to meet the demands of the CBB cycle (Allen, 2002; Kramer et al., 2004). Consequently, auxiliary electron transport (AET) plays a critical role in meeting the metabolic ATP requirements and regulating and protecting the photosynthetic apparatus, particularly under fluctuating environmental conditions. In cyclic electron transport (CET), Fd_{red} is oxidised either by the NDH-1 complex, also known as photosynthetic complex I, in several plant taxa and cyanobacteria, or by the pathway dependent on the PGRL1 and PGR5 proteins in plants and algae (Buchert et al., 2020;

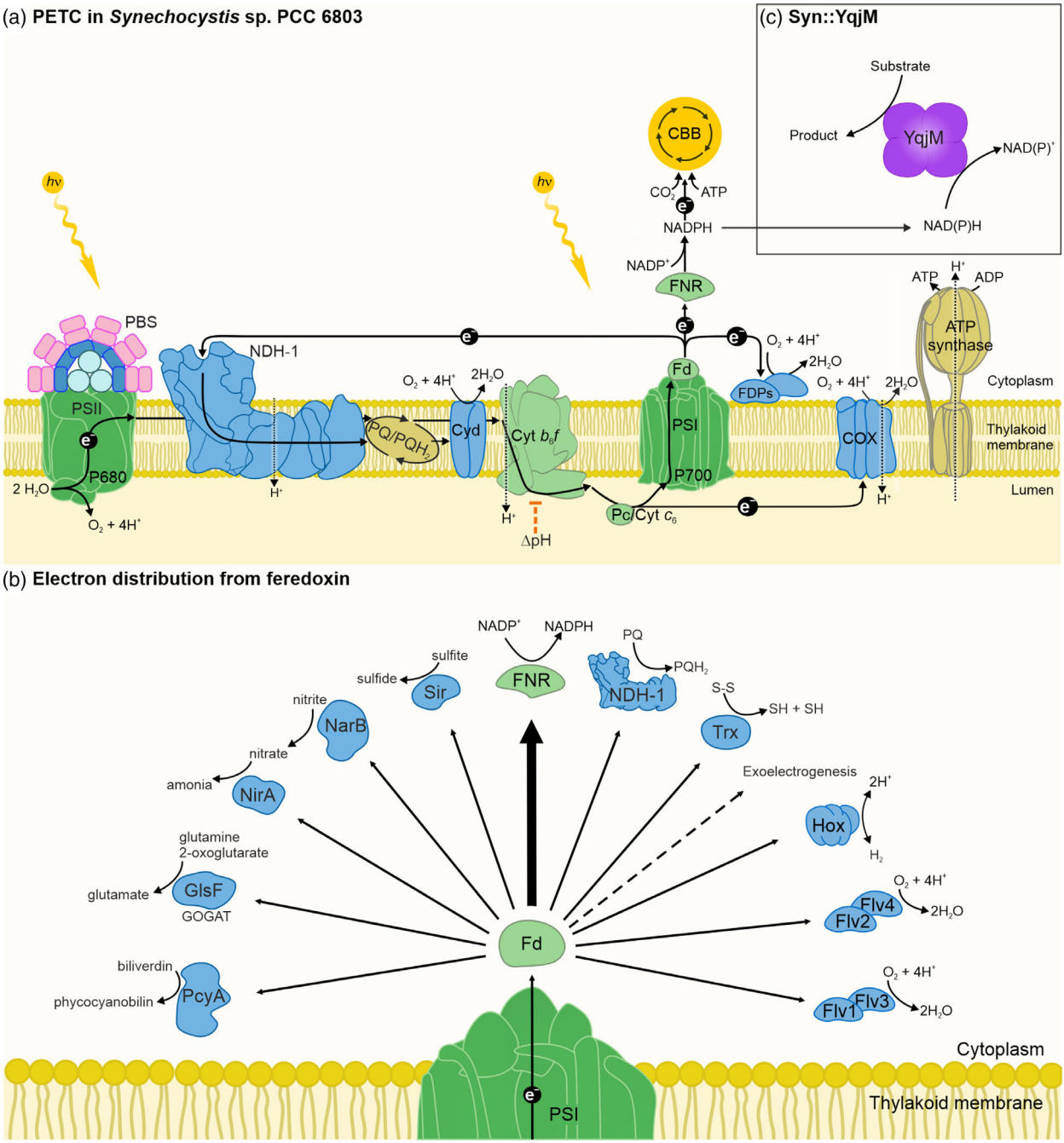

Figure 1. Photosynthetic electron transport chain (PETC) and electron distribution from Fd in the model cyanobacterium *Synechocystis* sp. PCC 6803.
(a) Simplified schematic of the PETC. The PETC in cyanobacteria consists of photosystem I and II (PSI and PSII, respectively), Cytochrome b_6f (Cyt b_6f) and electron carriers plastocyanin (Pc), Cytochrome c_6 (present under copper limitation) and ferredoxin (Fd). The last step of linear electron transport (LET) is the reduction of $NADP^+$ into NADPH by ferredoxin-NAD(P)H-oxidoreductase (FNR). NADPH is consumed by the Calvin–Benson–Bassham (CBB) cycle and other metabolic processes. Generated pmf is driving ATP synthesis. The cyclic electron transport (CET) around PSI is mediated by the NADH-dehydrogenase-like complex (NDH-1). RTOs cytochrome bd quinol oxidase (Cyd) and aa3-type cytochrome c oxidase (COX) reduce O_2 to water. Furthermore, flavodiiron proteins (FDPs), constituting a key photoprotective mechanism under fluctuating light conditions, have been lost in angiosperms and red and brown algae (Allahverdiyeva et al., 2015; Ilík et al., 2017; Peltier et al., 2010).
(b) The electron distribution from Fd. Fd_{red} serves as the electron donor for several pathways. The FDPs in heterooligomeric conformations Flv1/3 and Flv2/4 perform the Mehler-like reaction, reducing O_2 to water. The CET, mediated by NDH-1, shuffles electrons from Fd back to the PQ pool. Bidirectional hydrogenase (Hox) is involved in hydrogen metabolism. The thioredoxin (Trx) regulation system regulates, e.g. light-dependent activation of CBB enzymes. Other pathways include phycocyanobilin: ferredoxin oxidoreductase (PcyA), ferredoxin-dependent glutamate synthase (GlsF, GOGAT), ferredoxin-sulphite reductase (Sir), nitrate reductase (NarB) and nitrite reductase (NirA).
(c) *Synechocystis* sp. PCC 6803 expressing the gene of the NAD(P)H-accepting flavin-dependent oxidoreductase YqjM (Syn::YqjM).

DalCorso et al., 2008; Nikkanen et al., 2020; Peltier et al., 2016; Yadav et al., 2020).

Fd_{red} has been recently pinpointed as the electron donor for FDPs (Nikkanen et al., 2020, 2023; Sétif et al., 2020), which catalyse the photo-reduction of O_2 to water (Mehler-like reaction) upon sudden increases in light intensity in cyanobacteria, green algae and gymnosperms (Alboresi et al., 2019; Allahverdiyeva et al., 2013; Bag et al., 2022; Santana-Sanchez et al., 2019; Zhang et al., 2012). Fd_{red} also drives the assimilation of metabolites, such as nitrate and nitrite (Flores et al., 2005), and to a lesser extent, sulphite (Kaneko et al., 1996), glutamate (Navarro et al., 2000) and biliverdin (Frankenberg et al., 2001). Under specific conditions, some green algae and cyanobacteria employ hydrogenases to utilise Fd_{red} for hydrogen metabolism (Kosourov et al., 2021) and N_2-fixing cyanobacteria use Fd_{red} as the electron donor to nitrogenase (Magnuson & Cardona, 2016). Fd_{red} also provides reducing power for the thioredoxin system, which plays a crucial role in regulating various processes, including light-dependent activation of CBB enzymes (Mallén-Ponce et al., 2022). Finally, Fd has also been proposed as a potential electron exit point for photosynthetic microbes during exoelectrogenesis (Wey et al., 2019).

Photosynthetic reducing equivalents, Fd_{red} and NAD(P)H, can be harnessed as electron donors for heterologously expressed oxidoreductases to convert substrates into industrially relevant compounds through whole-cell photo-biotransformation (Jensen et al., 2011; Malihan-Yap et al., 2022; Schmermund et al., 2019). For example, NAD(P)H-dependent enzymes have been exploited for the oxyfunctionalisation of ketones into lactones (Erdem et al., 2022; Tüllinghoff et al., 2022) and for the reduction of maleimides (Assil-Companioni et al., 2020; Barone et al., 2023). Fd_{red} has supplied electrons to cytochrome P450s (Cyt P450), which offer a wide range of reactions (Agustinus & Gillam, 2023; Wlodarczyk et al., 2016). The effect of introducing these artificial electron sinks on the photosynthetic electron transport chain (PETC) has been partially explored. A recent study demonstrated that the heterologous expression of Cyt P450 in *Synechococcus elongatus* PCC 7942 led to enhancements in the quantum yield of photosystem II (PSII) and maximal oxidation of photosystem I (PSI) reaction centre chlorophylls (P700). Furthermore, a co-expression of carbon and electron sinks had a cumulative positive effect on photosynthetic yield (Santos-Merino et al., 2021).

Deleting natural electron sinks has gained popularity as an approach to enhance the yields of whole-cell biotransformation. However, the effects of such modifications on the PETC vary. A study using Cyt P450 showed an increase in electron transport through PSII by deleting a subunit of the NDH-1 complex, with no effects on PSI (Berepiki et al., 2018). Contrastingly, deleting the thylakoid-localised respiratory terminal oxidase (RTO), aa3-type cytochrome *c* oxidase (COX), led to an increase in electron transport mainly through PSI with a minor increase through PSII (Torrado et al., 2022). Deleting FDPs has also led to an increased biotransformation yield, with no or unclear effects on the PETC (Assil-Companioni et al., 2020; Erdem et al., 2022; Spasic et al., 2022). Such deletions improved the yield often only under specific conditions, indicating the complexity of cellular redox balance and suggesting that the improvements might not be a direct effect of rewiring the electron flux (Assil-Companioni et al., 2020; Santos-Merino et al., 2021; Spasic et al., 2022). A holistic overview of the photosynthetic apparatus and the dynamics of interaction between natural and artificial electron sinks is still missing.

Our primary aim was to elucidate the electron partitioning downstream of PSI and evaluate the effect of a strong artificial electron sink coupled to the photosynthetic light reactions. To achieve this, we combined analytical methods for monitoring the biotransformation reaction with real-time monitoring of O_2 gas fluxes for the first time. We used previously engineered cyanobacterium *Synechocystis* sp. PCC 6803 (hereafter *Synechocystis*), which heterologously expressed the gene for NAD(P)H-dependent ene-reductase YqjM, sourced from the non-photosynthetic bacterium *Bacillus subtilis* (Fitzpatrick et al., 2003). This recombinant enzyme catalyses the reduction of exogenously added 2-methylmaleimide (2-MM) into 2-methylsuccinimide (2-MS), enabling whole-cell biotransformation. This system has demonstrated fast conversion of 10 mM 2-MM within an hour (Assil-Companioni et al., 2020) and is presumed NAD(P)H-limited under photoautotrophic conditions (Barone et al., 2023).

We carried out a comprehensive analysis of the photosynthetic performance of YqjM-expressing cyanobacteria using a suite of state-of-the-art biophysical and biochemical techniques. This approach allowed us to reveal that the heterologous electron sink YqjM outcompetes the endogenous AET pathways downstream of PSI for photosynthetic reductants. This indicates that FNR is the preferred route of electrons from the Fd hub if FNR's activity is not limited by the availability of $NADP^+$ in the presence of YqjM enzyme and its substrate. Furthermore, YqjM consumed over half of the available photosynthetic electrons for the reduction of 2-MM and effectively prevented the transient pooling of electrons in the PETC. In addition to elucidating the fundamental aspects of the orchestration of photosynthetic electron flux, our findings lay the foundations for rational optimisation of whole-cell biotransformations and other applications that harness the reducing power of photosynthesis.

The Plant Journal published by Society for Experimental Biology and John Wiley & Sons Ltd.,
The Plant Journal, (2024), doi: 10.1111/tpj.16935

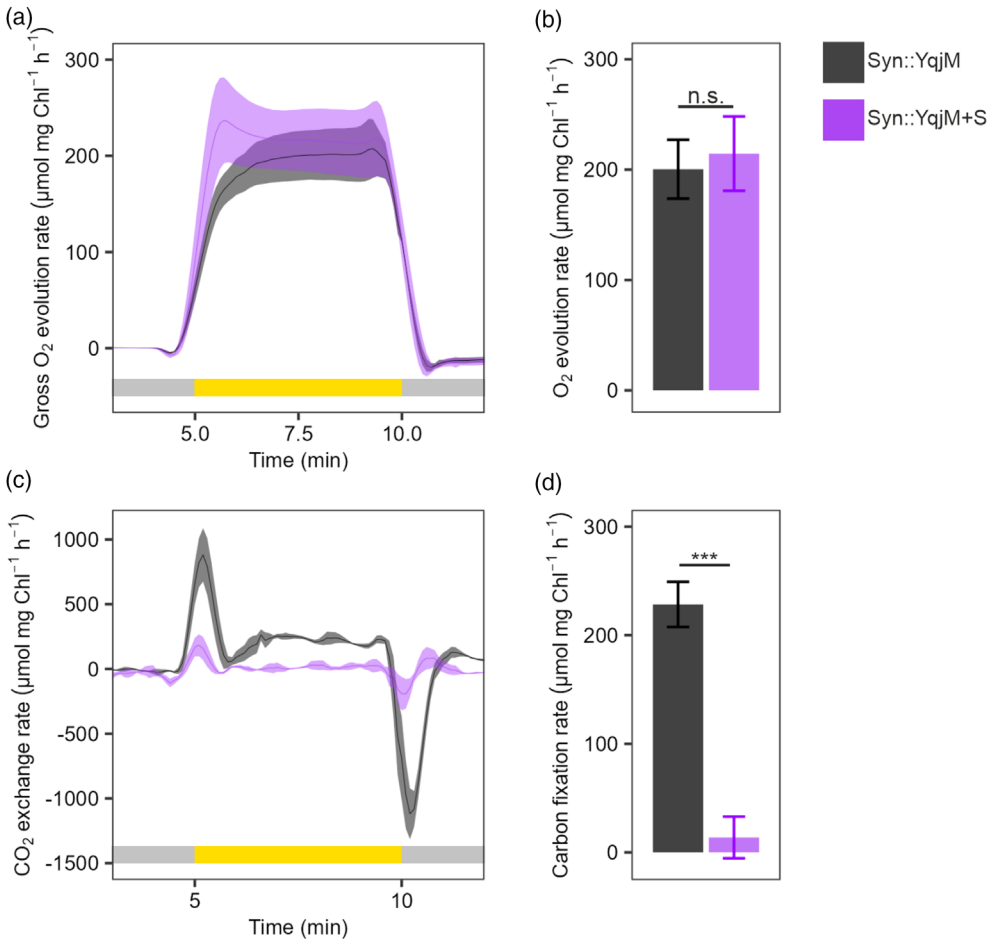

Figure 2. Gas exchange in Syn::YqjM ± S.
(a) Kinetics of gross O_2 evolution rate.
(b) Steady-state gross ($P = 9.05 \times 10^{-1}$) O_2 evolution rate.
(c) Kinetics of CO_2 exchange rate.
(d) Steady-state carbon fixation rate ($P = 1.03 \times 10^{-4}$). Rates are calculated from a 30 sec sliding window. Data presented as the mean of three biological replicates, error bars in column graphs or shading in traces are standard deviations. Statistical significance was tested by one-way ANOVA, n.s. >0.05, ***≤0.001. Black – Syn::YqjM, purple – Syn::YqjM + S, grey bar in (a, c) denotes darkness, yellow bar in (a, c) denotes illumination. For gas exchange in WT ± S, see Figure S3.

RESULTS

Active heterologous electron sink YqjM is a good tool for studying electron fluxes from Fd

In order to isolate the effects of the active heterologous electron sink on the photosynthetic electron fluxes in cyanobacteria, we confirmed that heterologously expressing YqjM in *Synechocystis* (Syn::YqjM) without the addition of the substrate has no effect on photosynthesis (Figure S2).

The addition of the substrate 2-MM (substrate, S, 10 mM final concentration) (Assil-Companioni et al., 2020; Köninger et al., 2016) to wild-type (WT) cells not expressing YqjM (WT + S) inhibited both gross and net O_2 evolution. However, in cells expressing YqjM (Syn::YqjM), the addition of the substrate (Syn::YqjM + S), while making the induction of O_2 evolution faster, did not alter steady-state O_2 evolution (Figure 2a,b; Figure S3a,b). Similarly, a decrease in the effective yield of PSII [Y(II)] and the electron transport rate through PSII [ETR(II)], as determined from SP analysis of Chl *a* fluorescence, was observed with addition of substrate to WT cells, but no change was observed for Syn::YqjM + S (Figure S4d,f). Considering the quantification of Y(II) and ETR(II) is performed under red AL, we tested Membrane Inlet Mass Spectroscopy (MIMS) using red AL of the same intensity (500 $\mu mol_{photons}$ m^{-2} sec^{-1}) and observed no changes compared to broad spectrum white light (Figure S5). This shows that active YqjM does not perturb the primary electron input into the PETC (water photo-oxidation by PSII). Consequently, it serves as a suitable tool for comparing the impact of active YqjM on photosynthetic electron fluxes in relation to WT. Additionally, the substrate

inhibited CO_2 fixation in both WT and Syn::YqjM cells (Figure 2c,d; Figure S6), which allowed us to examine AET centred around Fd (Figure 1b) isolated from interplay with the carbon metabolism. The addition of substrate to WT cells increased the ratio of O_2 photoreduction (indicating predominantly FDP activity) relative to gross O_2 evolution from 48 ± 7% to 81 ± 4% during the dark-to-light transition and from 20 ± 5% to 50 ± 6% at steady-state illumination, while the O_2 photoreduction rate slightly decreased (Figure S3c–e). Similarly, the CET:LET ratio more than doubled from 14 ± 4% to 35 ± 17% upon the addition of substrate to WT cells (Figure S7a). The number of electrons directed towards CET also increased fourfold (Figure S7b). These data indicate relatively greater electron distribution to AET pathways in the presence of the substrate in WT, possibly due to the lack of CO_2 fixation.

Interestingly, the substrate increases the proton conductivity of the thylakoid membrane in both WT and Syn::YqjM cells (Figure S8). This results in the dissipation of the *pmf* (Figure S8), preventing the induction of 'photosynthetic control' at Cyt b_6f. The substrate thereby unleashes photosynthesis for uninhibited electron flux to Fd.

Active heterologous electron sink YqjM outcompetes natural AET pathways

With active YqjM established as a tool for studying photosynthetic electron fluxes, we probed its effects on the electron distribution downstream of PSI considering Fd_{red} as the distribution hub (Figure 3a). YqjM converts supplied 2-MM to 2-MS within hours while oxidising NAD(P)H into $NAD(P)^+$ (Figure 1c). Syn::YqjM exhibited specific activity 116 ± 29 U g_{DCW}^{-1} [OD_{750} = 2.5, (Figure 3b)] comparable with previously reported values 166 ± 5 U g_{DCW}^{-1} [OD_{750} = 2, (Assil-Companioni et al., 2020)]. It is important to note that while NADH can also serve as the electron donor to YqjM, NADPH has a 3.5-fold higher affinity to YqjM (Assil-Companioni et al., 2020). YqjM maintains only residual activity in the dark, demonstrating a considerably lower reaction rate (Assil-Companioni et al., 2020). Upon illumination, YqjM efficiently utilised NADPH produced by the light reactions, as shown by the negligible light-induced accumulation of NADPH in Syn::YqjM + S (Figure 3c; Figure S9). Similarly, the Fd pool remained oxidised during illumination, as revealed by near-infrared absorbance difference measurements (Figure 3d), indicating efficient and continuous oxidation of Fd_{red}.

Next, we investigated if the AET pathways, reliant on Fd_{red} as their electron donor, contribute to Fd oxidation in Syn::YqjM + S. The activity of NDH-1 mediated CET was followed by the post-illumination increase in chlorophyll fluorescence (F_0 rise) and the CET:LET ratio was determined by analysing the dark-interval relaxation kinetics of the P700 and Pc redox change signals using the DUAL-KLAS-NIR (DKN) (Theune et al., 2021). While the F_0 rise was eliminated, the CET:LET ratio decreased sixfold from 19 ± 13% to 3 ± 1% in Syn::YqjM + S (Figure 3e). The O_2 photoreduction catalysed by FDPs was monitored by MIMS, using the enrichment of a heavy oxygen isotope ($^{18}O_2$) during real-time gas exchange measurements to distinguish O_2 evolution from consumption. With YqjM active and oxidising NAD(P)H, O_2 photoreduction decreased close to non-detectable values (Figure 3f). As a result, the ratio of O_2 photoreduction to gross O_2 evolution at the dark-to-light transition and steady-state illumination also strongly decreased (Figure S3d,e). Importantly, FDP accumulation levels were unchanged in Syn::YqjM compared to WT (Figure S10). These results suggest that when the $NADPH/NADP^+$ pool is kept oxidised by active YqjM in Syn::YqjM + S, the available Fd_{red} is primarily used by FNR for $NADP^+$ reduction.

The presence of the active YqjM as an electron sink in Syn::YqjM + S increases the PSI electron transport rate quantified by dark interval relaxation kinetics (DIRK) and saturating pulse (SP) analysis of P700 oxidation (Figure 4b; Figure S4c,e) despite the drop in CET contribution (Figure 4b). The strong oxidising effect of active YqjM on the PETC was further demonstrated by the absence of transient re-reduction of P700, the Cyt b_6f and the electron carrier Pc during the first seconds of illumination in Syn::YqjM + S (Figure 4c–f – dashed vertical line). As we use copper-replete media in this study, Pc is the main electron carrier between Cyt b_6f and PSI. The *b* hemes, Cyt *f* and Pc remained oxidised even after the illumination period (Figure 4c–e; Figure S11). The efficient oxidation of the PETC downstream of PSII (Cyt b_6f, Pc and P700) by the active YqjM allows for immediate induction of O_2 evolution upon illumination (Figure 2a).

Electron flux analysis: YqjM consumes more than half of the electrons released by PSII

With YqjM efficiently consuming available NADPH produced by the light reactions, we coupled the biotransformation reaction with real-time gas exchange measurements to quantify the flux of electrons from water oxidation to YqjM. After initiating the biotransformation process by introducing 10 mM of substrate to the cells, the reaction was monitored for 20 min, out of which 10 min were in light and 10 min in the dark in the 5–10–5 min of dark–light–dark regime (Figure S13). Subsequently, 0.69 ± 0.07 mM of the product, 2-MS, was detected. By subtracting the dark rate, which was calculated in a separate experiment, we determined that the light-dependent production was 0.45 ± 0.07 mM. Correspondingly, within the 10 min illumination period, we measured 0.41 ± 0.03 mM of total evolved O_2. Hence, the ratio of product formed to O_2 evolved was 1.09 ± 0.09. PSII oxidises two molecules of water into one molecule of O_2 through the extraction of four electrons from the water

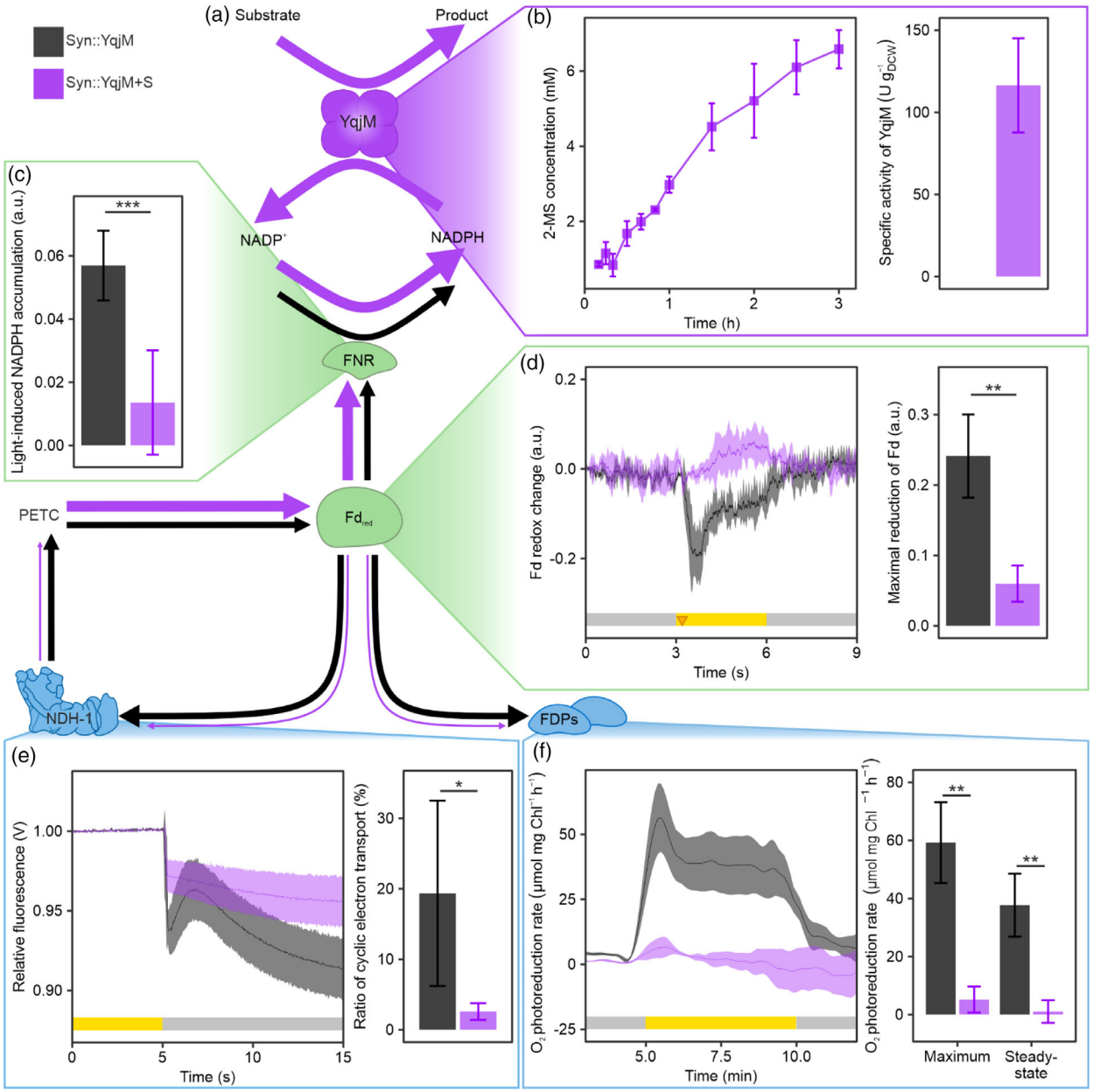

Figure 3. The electron distribution downstream of PSI in Syn::YqjM ± S.
(a) Schematic of electron flux. The black arrows signify Syn::YqjM, while the purple arrows signify Syn::YqjM + S. The arrows' thickness indicates the electron flow.
(b) Concentration of the product during the biotransformation reaction and specific activity of YqjM calculated from the first 20 min of biotransformation reaction.
(c) Light-induced accumulation of NADPH as the difference between NAD(P)H fluorescence level after and before illumination ($P = 6.85 \times 10^{-4}$).
(d) The kinetics of Fd redox state upon illumination and the maximal reduction of Fd upon illumination relative to the dark level ($P = 4.43 \times 10^{-3}$).
(e) The post-illumination F_0 rise in chlorophyll fluorescence normalised to steady-state fluorescence and the cyclic electron transport (CET) ratio ($P = 4.40 \times 10^{-2}$) assessed by dark-interval relaxation kinetics of P700 and Pc during illumination.
(f) The kinetics of O_2 photoreduction rate upon illumination and the maximal ($P = 1.40 \times 10^{-3}$) and steady-state ($P = 3.58 \times 10^{-3}$) O_2 photoreduction rate as a proxy for the activity of FDPs. Rates are calculated from a 30 sec sliding window. Data presented as the mean of three biological replicates [four in (c) and CET ratio in (e)], error bars in column graphs or shading in traces are standard deviations [standard error of the mean in (b) 2-MS concentration over time]. Black – Syn::YqjM, purple – Syn::YqjM + S, the grey bar denotes darkness and the yellow bar denotes illumination. Statistical significance was tested by one-way ANOVA, *≤0.05, **≤0.01, ***≤0.001.

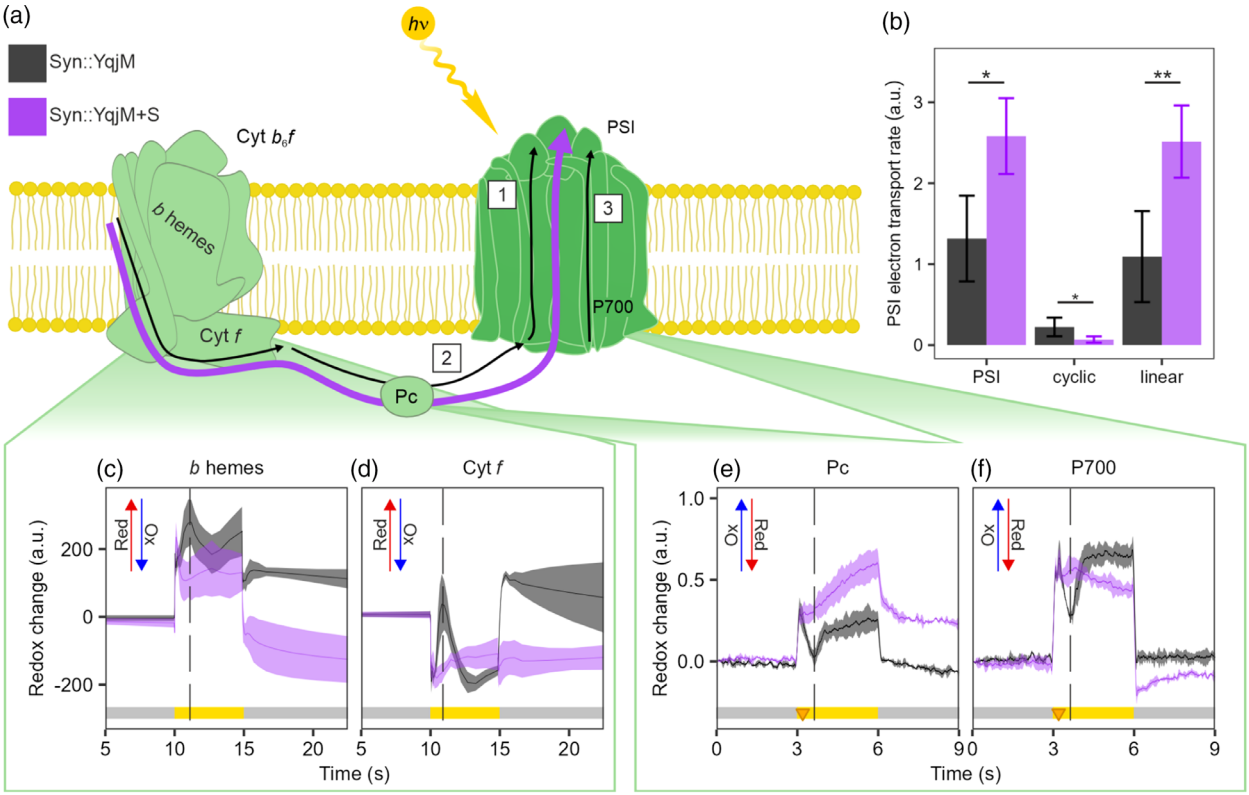

Figure 4. The redox state of the photosynthetic electron transport chain (PETC) and the electron transport through PSI in Syn::YqjM ± S.
(a) Schematic of the oxidation/reduction steps of the PETC upon illumination in Syn::YqjM − S (black) and Syn::YqjM + S (purple). (1) Oxidation of the PETC upon illumination, (2) The transient reduction caused by the inflow of electrons from PSII and the lack of available acceptors downstream of PSI and (3) The re-oxidation of the PETC when electron acceptors are available. In Syn::YqjM+S, no transient reduction is observed and the PETC is kept oxidised.
(b) Total electron transport through PSI with WT set to 1 ($P = 1.16 \times 10^{-2}$) and the individual cyclic ($P = 4.33 \times 10^{-2}$) and linear ($P = 7.44 \times 10^{-3}$) electron transport during steady-state illumination.
Redox signatures of Cyt b_6f components (c) b hemes and (d) Cyt *f*. See also Figure S12 for the Cyt b_6f redox signatures in WT ± S. The redox signature of (e) the electron carrier Pc and (f) PSI reaction centre chlorophylls P700. The triangle represents the time a saturating pulse (SP) was given to the sample. The dashed vertical line points at the transient reduction of P700, Pc, b hemes and Cyt *f*. The red arrow signifies reduction (Red), while the blue arrow signifies oxidation (Ox). The coloured bar in (b–e) signifies the illumination mode, grey – dark, yellow – illumination. Data presented as the mean of three biological replicates [four in (b)], error bars in column graphs or shading in traces are standard deviations [standard error of the mean in (c, d)]. Statistical significance was tested by one-way ANOVA, *≤0.05, **≤0.01.

molecules. On the other hand, two electrons are needed to produce each molecule of NADPH and YqjM uses one molecule of NADPH per one molecule of substrate. We, therefore, concluded that 54 ± 5% of the electrons released by O_2 evolution at PSII end up being used by YqjM for reduction of the substrate (Figure 5). As a small portion of the electrons from water oxidation is lost, for example, as heat due to inefficiencies in the PETC before Fd, YqjM consumes a major portion of the chemical energy available for downstream processes in the form of NADPH.

DISCUSSION

Orchestrating the distribution of photosynthetic reducing power from Fd is crucial for both photosynthetic organisms responding to change and the bioengineer re-directing photosynthetic reductants to desired reactions. However, the mechanisms determining the fate of electrons at the Fd distribution hub have remained largely elusive. Our results reveal that in the presence of the strong NAD(P)H-consuming heterologous sink, which maintains the NADPH/$NADP^+$ pool at an oxidised state (Figure 3c), the AET pathways of the Mehler-like reaction and CET are outcompeted for electrons from Fd (Figure 3e, f). This indicates that when the availability of the $NADP^+$ substrate is not limiting its activity, FNR is the preferred acceptor for electrons from Fd, pinpointing the cellular NADPH/$NADP^+$ ratio as a key factor in orchestrating photosynthetic electron flux. These findings have profound implications for rationally optimising the productivity of biotransformation platforms based on photosynthetic microbes and improving crop plants' yield and climate resilience.

While incremental advances in understanding how the distribution of photosynthetic reducing power from Fd_{red} is

(a)

Biotransformation coupled with MIMS

	Total product conc. (mM)	Dark rate (mM/min)	Light-dependent product (mM)	Specific activity (U/gDCW)	Specific activity (U/mg Chl)	Total evolved O_2 (mM)	Product to oxygen ratio (mol/mol)	Electron consumption (%)
YqjM+S	0.69 ± 0.07	0.01 ± 0	0.45 ± 0.07	143.61 ± 13.61	6.16 ± 0.91	0.41 ± 0.03	1.09 ± 0.09	54.3 ± 4.66

(b)

Figure 5. Electron flux towards active YqjM.
(a) Electron flux values derived from three independent biotransformation reactions performed in the MIMS sample chamber measuring the gas exchange followed by product concentration determination by GC.(b) Mapped electron flux originating from water oxidation towards biotransformation reaction compared to other end-processes.

controlled have previously been made, the underlying mechanisms have remained largely unknown. For example, *Synechocystis* has 11 Fd isoforms (Artz et al., 2020), but their specific bioenergetic roles are poorly understood. High-abundance Fd1 is the main isoform involved as the final electron acceptor in the PETC. We recently showed that it is also the main electron donor to FDP heterooligomers (Nikkanen et al., 2023). The low-abundance Fd isoforms 2–11 likely serve other condition-specific processes such as ROS scavenging systems (Cassier-Chauvat & Chauvat, 2014; Marteyn et al., 2009), the NiFe-hydrogenase (Gutekunst et al., 2014), nitrogen assimilation (Motomura et al., 2019), or mixotrophic carbon metabolism (Wang et al., 2022). Coordination of electron flux from Fd1 between FNR (and downstream carbon fixation) and the AET pathways is, therefore, the primary task in maintaining maximal photosynthetic efficiency without compromising photoprotection. However, besides the NADPH/$NADP^+$ ratio, other regulatory mechanisms likely also play a role in achieving dynamic coordination of electron flux and several influencing factors must be considered.

We showed that the addition of the 2-MM substrate achieves an uncoupled state of photosynthesis, as the *pmf* is dissipated due to the increased conductivity of the thylakoid membrane (Figure S8). The dissipation of the *pmf* means that photosynthetic control, i.e. inhibition of PQH_2 oxidation at Cyt b_6f at low lumenal pH (Malone et al., 2021), is not a limiting factor of YqjM biotransformation yield and optimisation strategies aiming at *pmf* uncoupling, for example by deletion of the inhibitory epsilon subunit of ATP synthase (Imashimizu et al., 2011) or by using ionophoric uncouplers, will not provide further benefit. Strategies to decrease the CO_2 fixation activity of CBB as a competitive NADPH sink will be ineffective, as the CBB is already inactive (Figure 2c,d; Figure S6), possibly due to disturbed redox regulation caused by the thiol-binding nature of 2-MM. The factor limiting biotransformation yield in Syn::YqjM is likely either water oxidation and consequent LET rate, or the capacity of FNR to reduce $NADP^+$ since all NADPH produced by FNR in light was efficiently consumed in the presence of active YqjM (Figure 3c). FNR activity may also be affected by *pmf* dissipation. In plant chloroplasts, the binding of FNR to its thylakoid anchor proteins is pH-dependent (Benz et al., 2010). While it is yet to be determined if *pmf* also controls the association of FNR to cyanobacterial phycobilisomes, FNR has been observed to disassociate from phycobilisomes in a low ionic strength buffer (Van Thor, 1999).

The association of FDP heterooligomers with the thylakoid membrane increases with the loss of *pmf*, likely enhancing the O_2 photoreduction activity (Nikkanen et al., 2023). Therefore, adding 2-MM should result in a

relative increase in O_2 photoreduction, which we observed in WT (Figure S3d,e). In Syn::YqjM, the lack of O_2 photoreduction in the presence of the substrate indicates that the exogenous NAD(P)H-consuming electron sink is able to outcompete FDPs despite the FDP-activating effect of the *pmf* dissipation. Similarly, the addition of 2-MM increased CET in WT (Figure S7) but not in Syn::YqjM + S (Figures 3e and 4b). This suggests that NDH-1 is outcompeted for electrons from Fd_{red} in the presence of active YqjM. In addition to the above-mentioned effects, 2-MM can potentially have other targets within the PETC (Appendix S1).

Interestingly, ETR(I) as measured by P700 spectroscopy and specifically electron transport rate through PSI as measured using NIR differential spectroscopy increased in the presence of active YqjM (Figure 4b; Figure S4c,e), while PSII O_2 evolution as measured by MIMS and ETR(II) as measured by Chl fluorescence did not (Figure 2a,b; Figure S4d, f). In simultaneous quantification of the electron transport rates through PSI and PSII there was a significant increase in the ETR(I)/ETR(II) ratio from 3.30 ± 0.07 in Syn::YqjM to 3.89 ± 0.22 in Syn::YqjM + S ($P = 6.9 \times 10^{-6}$, Figure S4a). A roughly 30% increase in electron transport rate through PSI with a minor effect on PSII was also observed in a *Synechococcus* strain lacking COX and expressing Cyt P450 (Torrado et al., 2022). Although the inhibition of thylakoid RTOs affected Y(II) and P700 oxidoreduction due to the accumulation of electrons in the PETC, the contribution of RTOs to O_2 photoreduction in *Synechocystis* is low (Ermakova et al., 2016; Viola et al., 2021). Therefore, it is not likely that the redirection of electrons from Pc towards PSI instead of COX is sufficient to account for the discrepancy in the PSI and PSII electron transport rates. The additional electrons to PSI also do not derive from CET or respiratory electrons from the cytosol as the presence of active YqjM resulted in the loss of CET as measured using the post-illumination increase in Chl fluorescence and NIR differential spectroscopy with [3-(3,4-dichlorophenyl)-1,1-dimethylurea] (DCMU) (Figures 3e and 4b) (Theune et al., 2021). Indeed, previous studies have pointed out the challenge of reliable quantification of simultaneous electron transfer rates (Fan et al., 2016; Kauny & Sétif, 2014). Furthermore, the various techniques used in our study may be affected differently by the biotransformation system. Therefore, multiple experimental approaches to measure the 'same' components of photosynthesis and building coupled systems for simultaneous measurements, as we have achieved with MIMS and biotransformation here (Figure 5; also Figure S4), is an essential approach for achieving a holistic understanding of bioenergetics.

YqjM effectively oxidised available NAD(P)H when supplied with 2-MM substrate. Previously, it has been estimated that YqjM consumes over 60% of NADPH produced by light reactions with a consumption of 680 μmol $mgChla^{-1}$ h^{-1} (Assil-Companioni et al., 2020). The estimated NADPH production in *Synechocystis* is 530–1070 μmol $mgChla^{-1}$ h^{-1} (Kauny & Sétif, 2014), demonstrating that YqjM can utilise most of the NADPH produced by FNR, depending on the specific conditions. Upon isolating the light-dependent production rate, we calculated that YqjM used over half of the electrons originating from water oxidation at PSII to reduce 2-MM into 2-MS (Figure 5), with the remaining electrons being lost due to inefficiencies in the PETC or consumed in other metabolic pathways downstream of PSI. It is important to note that there is uncertainty in these estimations and a discrepancy between rates of oxygen evolution and NADPH consumption has been reported (Kauny & Sétif, 2014). Nonetheless, our calculations indicate that a substantial portion of the reducing power produced by the photosynthetic light reactions is consumed by YqjM.

Targeting AET pathways has emerged as a popular strategy for increasing the product yield of whole-cell biotransformation applications (Assil-Companioni et al., 2020; Erdem et al., 2022; Jurkaš et al., 2022). Although the deletion of FDPs led to improved biotransformation yield (Assil-Companioni et al., 2020; Erdem et al., 2022), our results indicate that these enhancements are likely achieved indirectly rather than via the decreased competition for electrons from the PETC. Instead, for rational optimisation, we should focus on increasing the photosynthetic electron transport rate in the PETC, engineering the enzymatic activity, or targeting the localisation of the enzyme. Attaching native and heterologous enzymes to PSI or Fd has been shown to be successful with Cyt P450s (Lassen et al., 2014; Mellor et al., 2016) and hydrogenase (Appel et al., 2020). However, in these applications, Fd_{red} is the electron donor rather than NAD(P)H. A fusion of PSI, Fd and FNR enhanced the electron transport rate (Medipally et al., 2023), demonstrating that the localisation of heterologous enzymes is a promising target for optimisation. Another potential target is the NADPH/$NADP^+$ pool. Increasing its overall size by, e.g. enhancing the phosphorylation of NAD^+ by overexpressing NAD kinases (Ishikawa & Kawai-Yamada, 2019), could supply FNR with additional $NADP^+$, allowing it to utilise more Fd_{red}. Additionally, considering the effects of the substrate on the cell is of utmost importance when engineering a production strain for whole-cell biotransformation.

In conclusion, we demonstrate that the strong artificial electron sink outcompetes the natural electron valve, FDP-driven Mehler-like reaction and CET. These results suggest that with an oxidised NADPH/$NADP^+$ pool, FNR is the preferred route for electrons from Fd_{red}. Furthermore, the active YqjM utilises over half of the available electrons released by water oxidation at PSII, increases the electron transport rate through PSI and prevents the transient pooling of electrons in the PETC. Lastly, characterising the cell's response to electron sink engineering is an important

precondition to the rational optimisation of photosynthesis and production strains. We propose that when a strong NAD(P)H-dependent heterologous enzyme is taking electrons directly from the PETC, focusing on improving the overall efficiency of PETC, the enzyme's activity or localisation are superior strategies to the deletion of AET pathways.

MATERIALS AND METHODS

Strains and culturing conditions

Synechocystis sp. PCC 6803 was used as the WT control in this study. *Synechocystis* strain harbouring the gene coding for the YqjM enzyme under the control of *cpcB* promoter and the substrate 2-MM were used as described previously (Assil-Companioni et al., 2020). Photoautotrophic cultivation was performed in 30 ml of BG-11 medium (20 mM HEPES, pH = 7.5) in 100 ml Erlenmeyer flasks. The cultivation conditions were 30°C, ambient CO_2 (0.04%), 50 μmol photons m^{-2} sec^{-1} constant white illumination and orbital shaking at 115 rpm. Kanamycin (50 μg ml^{-1}) was used in pre-experimental and stock cultures. No antibiotic was present in the experimental cultures.

Biotransformation conditions

Before biotransformation, cells were harvested in the logarithmic growth phase by centrifugation (5000 ***g***, 8 min, room temperature) and adjusted to OD_{750} = 2.5 in fresh BG-11. Chlorophyll *a* (Chl *a*) concentration was quantified by extraction with 90% methanol. The extract was measured at OD_{665} and multiplied by 12.7 to obtain the final concentration in μg ml^{-1}. The biotransformation was initiated by the addition of the substrate under the conditions adapted from a previous study (Assil-Companioni et al., 2020), with these adjustments: illumination of 200 $\mu mol_{photons}$ m^{-2} sec^{-1} white light, 2-MM concentration 10 mM and 5 min of reaction time. After the 5 min biotransformation reaction, samples were taken for specific measurements described below. To calculate the specific activity of YqjM, the biotransformation was followed for 3 h with samples taken periodically, rapidly frozen in liquid nitrogen and stored at −80°C prior to gas chromatography (GC) analysis.

Membrane inlet mass spectrometry

The *in vivo* fluxes of $^{16}O_2$ (m/z = 32), $^{18}O_2$ (m/z = 36) and CO_2 (m/z = 44) were followed by built-in-house MIMS as described earlier (Mustila et al., 2016) with minor adjustments. The final Chl *a* concentration was ~6 μg ml^{-1}, the total dissolved inorganic carbon concentration was adjusted to 1.5 mM by adding $NaHCO_3$ and the illumination period was set to 5–5-5 min of dark–light–dark, respectively. During the sample preparation, samples were diluted to the appropriate Chl *a* concentration with fresh BG-11 and handled in darkness. The gas exchange rates were calculated as reported (Beckmann et al., 2009). A filter (LEE Filter, 106 Primary Red) was used to provide red actinic illumination. The light intensity was adjusted to 500 $\mu mol_{photons}$ m^{-2} sec^{-1}. The rates are calculated from a 30 sec sliding window, thus they appear to increase prior to the onset of illumination and decrease before the end of the illumination period.

Fluorescence and absorbance changes

Chl *a* fluorescence was followed with the DUAL-PAM 100 spectrophotometer (Walz, Effeltrich, Germany). After the biotransformation reaction, samples were dark adapted for 2 min before being exposed to 100 $\mu mol_{photons}$ m^{-2} sec^{-1} red actinic light (AL) for 240 sec, followed by another 240 sec of 170 $\mu mol_{photons}$ m^{-2} sec^{-1} red AL illumination. An additional 60 sec were recorded with no AL illumination to follow the dark relaxation of the fluorescence signal to observe the F_0 rise.

DUAL-KLAS-NIR (DKN) spectrophotometer (Walz) was used to follow the redox changes of Pc, P700 and Fd as described previously (Nikkanen et al., 2020). Briefly, absorbance changes between 780–820, 820–870, 840–965 and 870–965 nm were used to deconvolute the redox changes of Pc, P700 and Fd using differential model plots. A set of *Synechocystis* mutant strains was previously used to measure these differential model plots using scripts provided by the manufacturer (Nikkanen et al., 2020). Before the measurement, Chl *a* concentration was set to 10 μg ml^{-1} by adding fresh BG-11 and samples were dark adapted for 10 min. The redox changes were followed by the modified NIRMAX script supplied in the software package, which is made up of 3 sec red AL illumination (3400 $\mu mol_{photons}$ m^{-2} sec^{-1}) followed by 4 sec of the dark period and an additional 10 sec of far red-light illumination. A SP to fully reduce the Fd pool was introduced after 200 msec of red AL illumination. Due to copper-replete BG-11 medium, Pc is the dominant electron carrier from Cyt b_6f to PSI. Any Cyt c_6 present could have a minor effect on the Pc signal (Sétif et al., 2019).

NAD(P)H fluorescence was measured with the NADPH/9-AA module for DUAL-PAM-100 (Walz). Samples were diluted with BG-11 to reach Chl *a* concentration of 5 μg ml^{-1} and dark-adapted for 10 min. The light-induced NADPH accumulation was followed by 10 sec of dark period followed by 180 sec of red AL illumination (200 μmol m^{-2} sec^{-1}) and a minute-long dark period.

For simultaneous quantification of PSI and PSII fluxes [ETR(I) and ETR(II), respectively] we followed Chl *a* fluorescence and P700 absorbance changes using a DUAL-PAM spectrophotometer. After the biotransformation reaction, samples were dark-adapted for 10 min before being exposed to ~200 $\mu mol_{photons}$ m^{-2} sec^{-1} red AL for 120 sec. A SP (5000 $\mu mol_{photons}$ m^{-2} sec^{-1}, 500 msec) was distributed every 20 sec to calculate the effective yields of PSI and PSII [Y(I) and Y(II), respectively]. ETR(II) and ETR(I) were calculated as follows: ETR(II) = Y(II) × PAR × 0.5 × 0.84 and ETR(I) = Y(I) × PAR × 0.5 × 0.84, where PAR is the photosynthetically active radiation (in $\mu mol_{photons}$ m^{-2} sec^{-1}), 0.84 is the proportion of photons absorbed by the cells and 0.5 is a correction factor assuming that photons are absorbed equally by PSII and PSI (Baker et al., 2007).

Redox changes of Cyt *f* and *b* hemes

The redox changes of Cyt *f* and *b* hemes of the Cyt b_6f complex were deconvoluted from the absorbance changes at 546, 554, 563 and 573 nm measured with the JTS-10 spectrophotometer (Bio-Logic, Seyssinet-Pariset, France), appropriate 10 nm full width at half-maximal interference filters (EdmundOptics, Barrington, NJ, USA) and BG39 filters (Schott, Mainz, Germany) protecting the light detectors from scattering effects. The samples were adjusted to Chl *a* concentration of 5 μg ml^{-1} and dark-adapted for 3 min prior to measurement with each filter. Then, they were illuminated for 5 sec with 500 $\mu mol_{photons}$ m^{-2} sec^{-1} green AL and white detection flashes were administered during 200 μsec dark intervals.

CET ratio quantification

Linear and CET rates were quantified by measuring DIRK of the P700 and Pc signals using the DKN, as described previously (Theune et al., 2021). The samples were adjusted to Chl *a* concentration of 15 μg ml^{-1}, Briefly, cells were pre-illuminated for 2 min under 500 $\mu mol_{photons}$ m^{-2} sec^{-1}, after which the light was

repeatedly (100×) shut off for 20 msec. The signals were averaged and the electron flow through PSI was calculated. Samples were measured in the presence and absence of 20 μM DCMU.

Calculating *pmf* from electrochromic shift measurement

The electrochromic shift (ECS) was measured as described previously (Nikkanen et al., 2020). Briefly, samples were set to a final Chl *a* concentration of 7.5 μg ml^{-1} and dark-adapted prior to exposure to 500 $\mu mol_{photons}$ m^{-2} sec^{-1} green AL interrupted with dark intervals. *pmf* was calculated as the extent of ECS decrease at the dark intervals. Thylakoid conductivity (gH^+) was calculated as the inverse of the time constant of a first-order fit to ECS relaxation kinetics during a dark interval and proton flux (vH^+) as *pmf* × gH^+ (Cruz et al., 2005).

Biotransformation coupled with MIMS

The sample was set in the MIMS sample chamber as described in MIMS methods above with the following modifications. The Chl *a* concentration was set to 11 ± 1 μg ml^{-1} and the final sample volume was 1 ml. The substrate was added to the final concentration of 10 mM and the measurement was started by 5 min dark-adaptation followed by 10 min of illumination (200 $\mu mol_{photons}$ m^{-2} sec^{-1}) and 5 min of a dark period. The reaction was stopped by rapidly freezing the sample in liquid nitrogen and the samples were stored at −80°C until GC analysis. The dark rate was calculated from a reaction set up in complete darkness for 1 h in otherwise the same conditions.

GC analysis

Samples were extracted using three-step extraction with ethyl acetate. The organic phase was dried using anhydrous $MgSO_4$ and analysed on GC-2010 Pro gas chromatograph (Shimadzu, Japan) equipped with an HP-5MS 30 m × 0.25 mm (5%-Phenyl)-methylpolysiloxane column (19091S-133; Agilent, Santa Clara, CA, USA) with nitrogen as the carrier gas with splitless injection mode. Compounds were separated at 35°C (hold 3 min), 200°C (hold 3 min, 10°C min^{-1}) and 300°C (hold 3 min, 25°C min^{-1}). Linear velocity was 11 cm sec^{-1}. Acetophenone was used as the internal standard. Calibration was performed with known amounts of 2-MM and 2-MS.

Protein extraction and immunoblotting

Total protein extracts from cultures were isolated as previously described (Zhang et al., 2009), separated by sodium dodecyl sulfate-polyacrylamide gel electrophoresis on BioRad Mini-PROTEAN TGX 4–15% precast gels with 6 M urea and blotted on polyvinylidene fluoride membranes. Membranes were probed with custom polyclonal antibodies raised against Flv1, Flv2, Flv3 and Flv4 (GenScript, Piscataway, NJ, USA). Horseradish peroxidase-conjugated secondary antibody (GE Healthcare, Chicago, IL, USA) and Amersham ECL (GE Healthcare) were used for detection.

Statistical analysis

Analysis and visualisation were conducted using R statistical software (R Core Team, 2020) and Origin (Version 2016) (Origin, 2016). Two-way ANOVA was used to test for significance. Tukey's test was used to compare the means of different groups with each other, with $P < 0.05$ as the significance cut-off.

Spectra measurement

The light spectra were measured using SpectraPen (PSI, Czech Republic) under the same conditions used in experiments – 500 $\mu mol_{photons}$ m^{-2} sec^{-1}. Spectra for MIMS and DKN instruments are shown in Figure S1.

AUTHOR CONTRIBUTIONS

YA conceived the study. MH, LN and YA designed the research. MH and LN performed the experiments. MH, LTW and LN analysed the data. MH, LTW, LN and YA interpreted the results and formed conclusions. LM-Y and RK provided the custom-made substrate and Syn::YqjM strain. YA secured funding. MH drafted the manuscript and all authors finalised and approved it.

ACKNOWLEDGEMENTS

This work was supported by the Academy of Finland (AlgaLEAF, project no. 322754, to YA; Revisiting Photosynthesis, project no. 315119, to YA), the Novo Nordisk Foundation (PhotoCat, project no. NNF20OC0064371, to YA) and the EU FET Open project FuturoLEAF (grant agreement No. 899576, to YA). All the experiments were performed within the PHOTOSYN infrastructure at the University of Turku. Linda Nevala is thanked for technical assistance with immunoblotting.

CONFLICT OF INTEREST

The authors declare no competing interests.

DATA AVAILABILITY STATEMENT

The datasets analysed during the current study are available from the corresponding author upon reasonable request.

SUPPORTING INFORMATION

Additional Supporting Information may be found in the online version of this article.

Figure S1. Spectra of the actinic light (AL) used in MIMS (broad white light) and DKN (623 nm red light).

Figure S2. Effect of the expression of YqjM in Synechocystis (WT and Syn::YqjM).

Figure S3. Effect of the substrate on the O_2 exchange rate in WT ± S and Syn::YqjM ± S.

Figure S4. Simultaneous quantification of electron fluxes through PSI and PSII.

Figure S5. The O_2 exchange rate upon illumination with red or white light in Syn::YqjM ± S.

Figure S6. CO_2 exchange rate in WT ± S.

Figure S7. Electron transport through PSI in WT ± S and Syn::YqjM ± S.

Figure S8. The effect of substrate on pmf generation in WT ± S and Syn::YqjM ± S.

Figure S9. Kinetics of NADPH fluorescence upon illumination by red actinic light (AL).

Figure S10. Immunodetection of FDP accumulation levels in WT and Syn::YqjM in the absence of the substrate.

Figure S11. The level of reduction of b hemes and Cyt *f* after the illumination period in Syn::YqjM ± S.

Figure S12. The redox signatures of Cyt b_6f in WT ± S.

Figure S13. The O_2 exchange rate during the biotransformation reaction run in the MIMS sample chamber.

Appendix S1. Effect of 2-MM on the thioredoxins system and electron transport.

REFERENCES

Agustinus, B. & **Gillam, E.M.J.** (2023) Solar-powered P450 catalysis: engineering electron transfer pathways from photosynthesis to P450s. *Journal of Inorganic Biochemistry*, **245**, 112242. Available from: https://doi.org/10.1016/j.jinorgbio.2023.112242

Alboresi, A., **Storti, M.** & **Morosinotto, T.** (2019) Balancing protection and efficiency in the regulation of photosynthetic electron transport across plant evolution. *The New Phytologist*, **221**, 105–109. Available from: https://doi.org/10.1111/nph.15372

Allahverdiyeva, Y., **Aro, E.-M.**, **van Bavel, B.**, **Escudero, C.**, **Funk, C.**, **Heinonen, J.** ***et al.*** (2021) NordAqua, a Nordic Center of Excellence to develop an algae-based photosynthetic production platform. *Physiologia Plantarum*, **173**, 507–513. Available from: https://doi.org/10.1111/ppl.13394

Allahverdiyeva, Y., **Mustila, H.**, **Ermakova, M.**, **Bersanini, L.**, **Richaud, P.**, **Ajlani, G.** ***et al.*** (2013) Flavodiiron proteins Flv1 and Flv3 enable cyanobacterial growth and photosynthesis under fluctuating light. *Proceedings of the National Academy of Sciences of the United States of America*, **110**, 4111–4116. Available from: https://doi.org/10.1073/pnas.1221194110

Allahverdiyeva, Y., **Suorsa, M.**, **Tikkanen, M.** & **Aro, E.-M.** (2015) Photoprotection of photosystems in fluctuating light intensities. *Journal of Experimental Botany*, **66**, 2427–2436. Available from: https://doi.org/10.1093/jxb/eru463

Allen, J.F. (2002) Photosynthesis of ATP—electrons, proton pumps, rotors, and poise. *Cell*, **110**, 273–276. Available from: https://doi.org/10.1016/S0092-8674(02)00870-X

Appel, J., **Hueren, V.**, **Boehm, M.** & **Gutekunst, K.** (2020) Cyanobacterial in vivo solar hydrogen production using a photosystem I–hydrogenase (PsaD-HoxYH) fusion complex. *Nature Energy*, **5**, 458–467. Available from: https://doi.org/10.1038/s41560-020-0609-6

Artz, J.H., **Tokmina-Lukaszewska, M.**, **Mulder, D.W.**, **Lubner, C.E.**, **Gutekunst, K.**, **Appel, J.** ***et al.*** (2020) The structure and reactivity of the Hox-EFU complex from the cyanobacterium Synechocystis sp. PCC 6803. *The Journal of Biological Chemistry*, **295**, 9445–9454. Available from: https://doi.org/10.1074/jbc.RA120.013136

Assil-Companioni, L., **Büchsenschütz, H.C.**, **Solymosi, D.**, **Dyczmons-Nowaczyk, N.G.**, **Bauer, K.K.F.**, **Wallner, S.** ***et al.*** (2020) Engineering of NADPH supply boosts photosynthesis-driven biotransformations. *ACS Catalysis*, **10**, 11864–11877. Available from: https://doi.org/10.1021/acscatal.0c02601

Bag, P., **Shutova, T.**, **Shevela, D.**, **Lihavainen, J.**, **Nanda, S.**, **Ivanov, A.G.** ***et al.*** (2022) O_2 photoreduction at acceptor side of photosystem I provide photoprotection to conifer thylakoids in early spring. *bioRxiv*. Available from: https://doi.org/10.1101/2022.10.21.513261

Baker, N.R., **Harbinson, J.** & **Kramer, D.M.** (2007) Determining the limitations and regulation of photosynthetic energy transduction in leaves. *Plant, Cell & Environment*, **30**, 1107–1125. Available from: https://doi.org/10.1111/j.1365-3040.2007.01680.x

Barbosa, M.J., **Janssen, M.**, **Südfeld, C.**, **D'Adamo, S.** & **Wijffels, R.H.** (2023) Hypes, hopes, and the way forward for microalgal biotechnology. *Trends in Biotechnology*, **41**, 452–471. Available from: https://doi.org/10.1016/j.tibtech.2022.12.017

Barone, G.D., **Hubáček, M.**, **Malihan-Yap, L.**, **Grimm, H.C.**, **Nikkanen, L.**, **Pacheco, C.C.** ***et al.*** (2023) Towards the rate limit of heterologous biotechnological reactions in recombinant cyanobacteria. *Biotechnology for Biofuels and Bioproducts*, **16**, 4. Available from: https://doi.org/10.1186/s13068-022-02237-4

Beckmann, K., **Messinger, J.**, **Badger, M.R.**, **Wydrzynski, T.** & **Hillier, W.** (2009) On-line mass spectrometry: membrane inlet sampling. *Photosynthesis Research*, **102**, 511–522. Available from: https://doi.org/10.1007/s11120-009-9474-7

Benz, J.P., **Stengel, A.**, **Lintala, M.**, **Lee, Y.-H.**, **Weber, A.**, **Philippar, K.** ***et al.*** (2010) *Arabidopsis* Tic62 and ferredoxin-NADP(H) oxidoreductase form light-regulated complexes that are integrated into the chloroplast redox poise. *Plant Cell*, **21**, 3965–3983. Available from: https://doi.org/10.1105/tpc.109.069815

Berepiki, A., **Gittins, J.R.**, **Moore, C.M.** & **Bibby, T.S.** (2018) Rational engineering of photosynthetic electron flux enhances light-powered cytochrome P450 activity. *Synthetic Biology*, **3**, ysy009. Available from: https://doi.org/10.1093/synbio/ysy009

Buchert, F., **Mosebach, L.**, **Gäbelein, P.** & **Hippler, M.** (2020) PGR5 is required for efficient Q cycle in the cytochrome *b* 6 *f* complex during cyclic electron flow. *The Biochemical Journal*, **477**, 1631–1650. Available from: https://doi.org/10.1042/BCJ20190914

Cassier-Chauvat, C. & **Chauvat, F.** (2014) Function and regulation of ferredoxins in the cyanobacterium, *Synechocystis* PCC6803: recent advances. *Life*, **4**, 666–680. Available from: https://doi.org/10.3390/life4040666

Cruz, J.A., **Kanazawa, A.**, **Treff, N.** & **Kramer, D.M.** (2005) Storage of light-driven transthylakoid proton motive force as an electric field ($\Delta\psi$) under steady-state conditions in intact cells of *Chlamydomonas reinhardtii*. *Photosynthesis Research*, **85**, 221–233. Available from: https://doi.org/10.1007/s11120-005-4731-x

DalCorso, G., **Pesaresi, P.**, **Masiero, S.**, **Aseeva, E.**, **Schünemann, D.**, **Finazzi, G.** ***et al.*** (2008) A complex containing PGRL1 and PGR5 is involved in the switch between linear and cyclic electron flow in Arabidopsis. *Cell*, **132**, 273–285. Available from: https://doi.org/10.1016/j.cell.2007.12.028

Erdem, E., **Malihan-Yap, L.**, **Assil-Companioni, L.**, **Grimm, H.**, **Barone, G.D.**, **Serveau-Avesque, C.** ***et al.*** (2022) Photobiocatalytic oxyfunctionalization with high reaction rate using a Baeyer–Villiger monooxygenase from *Burkholderia xenovorans* in metabolically engineered cyanobacteria. *ACS Catalysis*, **12**, 66–72. Available from: https://doi.org/10.1021/acscatal.1c04555

Ermakova, M., **Huokko, T.**, **Richaud, P.**, **Bersanini, L.**, **Howe, C.J.**, **Lea-Smith, D.J.** ***et al.*** (2016) Distinguishing the roles of thylakoid respiratory terminal oxidases in the cyanobacterium *Synechocystis* sp. PCC 6803. *Plant Physiology*, **171**, 1307–1319. Available from: https://doi.org/10.1104/pp.16.00479

Fan, D.-Y., **Fitzpatrick, D.**, **Oguchi, R.**, **Ma, W.**, **Kou, J.** & **Chow, W.S.** (2016) Obstacles in the quantification of the cyclic electron flux around photosystem I in leaves of C3 plants. *Photosynthesis Research*, **129**, 239–251. Available from: https://doi.org/10.1007/s11120-016-0223-4

Fitzpatrick, T.B., **Amrhein, N.** & **Macheroux, P.** (2003) Characterization of YqjM, an old yellow enzyme homolog from Bacillus subtilis involved in the oxidative stress response. *The Journal of Biological Chemistry*, **278**, 19891–19897. Available from: https://doi.org/10.1074/jbc.M211778200

Flores, E., **Frías, J.E.**, **Rubio, L.M.** & **Herrero, A.** (2005) Photosynthetic nitrate assimilation in cyanobacteria. *Photosynthesis Research*, **83**, 117–133. Available from: https://doi.org/10.1007/s11120-004-5830-9

Frankenberg, N., **Mukougawa, K.**, **Kohchi, T.** & **Lagarias, J.C.** (2001) Functional genomic analysis of the HY2 family of ferredoxin-dependent Bilin reductases from oxygenic photosynthetic organisms. *Plant Cell*, **13**, 965–978. Available from: https://doi.org/10.1105/tpc.13.4.965

Goss, T. & **Hanke, G.** (2014) The end of the line: can ferredoxin and ferredoxin NADP(H) oxidoreductase determine the fate of photosynthetic electrons? *Current Protein & Peptide Science*, **15**, 385–393.

Gutekunst, K., **Chen, X.**, **Schreiber, K.**, **Kaspar, U.**, **Makam, S.** & **Appel, J.** (2014) The bidirectional NiFe-hydrogenase in *Synechocystis* sp. PCC 6803 is reduced by flavodoxin and ferredoxin and is essential under mixotrophic, nitrate-limiting conditions. *The Journal of Biological Chemistry*, **289**, 1930–1937. Available from: https://doi.org/10.1074/jbc.M113.526376

Hanke, G. & **Mulo, P.** (2013) Plant type ferredoxins and ferredoxin-dependent metabolism. *Plant, Cell & Environment*, **36**, 1071–1084. Available from: https://doi.org/10.1111/pce.12046

Hitchcock, A., **Hunter, C.N.**, **Sobotka, R.**, **Komenda, J.**, **Dann, M.** & **Leister, D.** (2022) Redesigning the photosynthetic light reactions to enhance photosynthesis – the *PhotoRedesign* consortium. *The Plant Journal*, **109**, 23–34. Available from: https://doi.org/10.1111/tpj.15552

Ilík, P., **Pavlovič, A.**, **Kouřil, R.**, **Alboresi, A.**, **Morosinotto, T.**, **Allahverdiyeva, Y.** ***et al.*** (2017) Alternative electron transport mediated by flavodiiron proteins is operational in organisms from cyanobacteria up to gymnosperms. *The New Phytologist*, **214**, 967–972. Available from: https://doi.org/10.1111/nph.14536

Imashimizu, M., **Bernát, G.**, **Sunamura, E.-I.**, **Broekmans, M.**, **Konno, H.**, **Isato, K.** ***et al.*** (2011) Regulation of F0F1-ATPase from Synechocystis sp. PCC 6803 by γ and $\in$ subunits is significant for light/dark adaptation. *The Journal of Biological Chemistry*, **286**, 26595–26602. Available from: https://doi.org/10.1074/jbc.M111.234138

Ishikawa, Y. & **Kawai-Yamada, M.** (2019) Physiological significance of NAD kinases in cyanobacteria. *Frontiers in Plant Science*, **10**, 847.

Jensen, K., **Jensen, P.E.** & **Møller, B.L.** (2011) Light-driven cytochrome P450 hydroxylations. *ACS Chemical Biology*, **6**, 533–539. Available from: https://doi.org/10.1021/cb100393j

Jurkaš, V., **Winkler, C.K.**, **Poschenrieder, S.**, **Oliveira, P.**, **Pacheco, C.C.**, **Ferreira, E.A.** ***et al.*** (2022) Expression and activity of heterologous hydroxyisocaproate dehydrogenases in *Synechocystis* sp. PCC 6803 ΔhoxYH. *Engineering Microbiology*, **2**, 100008. Available from: https://doi.org/10.1016/j.engmic.2021.100008

Kaneko, T., **Sato, S.**, **Kotani, H.**, **Tanaka, A.**, **Asamizu, E.**, **Nakamura, Y.** ***et al.*** (1996) Sequence analysis of the genome of the unicellular cyanobacterium *Synechocystis* sp. strain PCC6803. II. Sequence determination of the entire genome and assignment of potential protein-coding regions. *DNA Research*, **3**, 109–136. Available from: https://doi.org/10.1093/dnares/3.3.109

Kauny, J. & **Sétif, P.** (2014) NADPH fluorescence in the cyanobacterium *Synechocystis* sp. PCC 6803: a versatile probe for in vivo measurements of rates, yields and pools. *Biochimica et Biophysica Acta (BBA) - Bioenergetics*, **1837**, 792–801. Available from: https://doi.org/10.1016/j.bbabio.2014.01.009

Köninger, K., **Gómez Baraibar, Á.**, **Mügge, C.**, **Paul, C.E.**, **Hollmann, F.**, **Nowaczyk, M.M.** ***et al.*** (2016) Recombinant cyanobacteria for the asymmetric reduction of C=C bonds fueled by the biocatalytic oxidation of water. *Angewandte Chemie, International Edition*, **55**, 5582–5585. Available from: https://doi.org/10.1002/anie.201601200

Kosourov, S., **Böhm, M.**, **Senger, M.**, **Berggren, G.**, **Stensjö, K.**, **Mamedov, F.** ***et al.*** (2021) Photosynthetic hydrogen production: novel protocols, promising engineering approaches and application of semi-synthetic hydrogenases. *Physiologia Plantarum*, **173**, 555–567. Available from: https://doi.org/10.1111/ppl.13428

Kramer, D.M., **Avenson, T.J.** & **Edwards, G.E.** (2004) Dynamic flexibility in the light reactions of photosynthesis governed by both electron and proton transfer reactions. *Trends in Plant Science*, **9**, 349–357. Available from: https://doi.org/10.1016/j.tplants.2004.05.001

Lassen, L.M., **Nielsen, A.Z.**, **Olsen, C.E.**, **Bialek, W.**, **Jensen, K.**, **Møller, B.L.** ***et al.*** (2014) Anchoring a plant cytochrome P450 via PsaM to the thylakoids in *Synechococcus* sp. PCC 7002: evidence for light-driven biosynthesis. *PLoS One*, **9**, e102184. Available from: https://doi.org/10.1371/journal.pone.0102184

Magnuson, A. & **Cardona, T.** (2016) Thylakoid membrane function in heterocysts. Organization and dynamics of bioenergetic systems in bacteria. *Biochimica et Biophysica Acta (BBA) - Bioenergetics*, **1857**, 309–319. Available from: https://doi.org/10.1016/j.bbabio.2015.10.016

Malihan-Yap, L., **Grimm, H.C.** & **Kourist, R.** (2022) Recent advances in cyanobacterial biotransformations. *Chemie Ingenieur Technik*, **94**, 1628–1644. Available from: https://doi.org/10.1002/cite.202200077

Mallén-Ponce, M.J., **Huertas, M.J.** & **Florencio, F.J.** (2022) Exploring the diversity of the thioredoxin systems in cyanobacteria. *Antioxidants*, **11**, 654. Available from: https://doi.org/10.3390/antiox11040654

Malone, L.A., **Proctor, M.S.**, **Hitchcock, A.**, **Hunter, C.N.** & **Johnson, M.P.** (2021) Cytochrome b6f – orchestrator of photosynthetic electron transfer. *Biochimica et Biophysica Acta (BBA) - Bioenergetics*, **1862**, 148380. Available from: https://doi.org/10.1016/j.bbabio.2021.148380

Marteyn, B., **Domain, F.**, **Legrain, P.**, **Chauvat, F.** & **Cassier-Chauvat, C.** (2009) The thioredoxin reductase-glutaredoxins-ferredoxin crossroad pathway for selenate tolerance in *Synechocystis* PCC6803. *Molecular Microbiology*, **71**, 520–532. Available from: https://doi.org/10.1111/j.1365-2958.2008.06550.x

Medipally, H., **Mann, M.**, **Kötting, C.**, **Van Berkel, W.J.H.** & **Nowaczyk, M.** (2023) A clickable photosystem I, ferredoxin, and ferredoxin NADP+ reductase fusion system for light-driven NADPH regeneration. *Chembiochem*, **24**, e202300025. Available from: https://doi.org/10.1002/cbic.202300025

Mellor, S.B., **Nielsen, A.Z.**, **Burow, M.**, **Motawia, M.S.**, **Jakubauskas, D.**, **Møller, B.L.** ***et al.*** (2016) Fusion of ferredoxin and cytochrome P450 enables direct light-driven biosynthesis. *ACS Chemical Biology*, **11**, 1862–1869. Available from: https://doi.org/10.1021/acschembio.6b00190

Motomura, T., **Zuccarello, L.**, **Sétif, P.**, **Boussac, A.**, **Umena, Y.**, **Lemaire, D.** ***et al.*** (2019) An alternative plant-like cyanobacterial ferredoxin with unprecedented structural and functional properties. *Biochimica et Biophysica Acta (BBA) - Bioenergetics*, **1860**, 148084. Available from: https://doi.org/10.1016/j.bbabio.2019.148084

Mullineaux, C.W. (2014) Co-existence of photosynthetic and respiratory activities in cyanobacterial thylakoid membranes. Dynamic and ultrastructure of bioenergetic membranes and their components. *Biochimica et Biophysica Acta (BBA) - Bioenergetics*, **1837**, 503–511. Available from: https://doi.org/10.1016/j.bbabio.2013.11.017

Mustila, H., **Paananen, P.**, **Battchikova, N.**, **Santana-Sánchez, A.**, **Muth-Pawlak, D.**, **Hagemann, M.** ***et al.*** (2016) The flavodiiron protein Flv3 functions as a homo-oligomer during stress acclimation and is distinct from the Flv1/Flv3 hetero-oligomer specific to the O_2 photoreduction pathway. *Plant & Cell Physiology*, **57**, 1468–1483. Available from: https://doi.org/10.1093/pcp/pcw047

Navarro, F., **Martín-Figueroa, E.**, **Candau, P.** & **Florencio, F.J.** (2000) Ferredoxin-dependent iron–sulfur flavoprotein glutamate synthase (GlsF) from the cyanobacterium *Synechocystis* sp. PCC 6803: expression and assembly in *Escherichia coli*. *Archives of Biochemistry and Biophysics*, **379**, 267–276. Available from: https://doi.org/10.1006/abbi.2000.1894

Nikkanen, L., **Santana Sánchez, A.**, **Ermakova, M.**, **Rögner, M.**, **Cournac, L.** & **Allahverdiyeva, Y.** (2020) Functional redundancy between flavodiiron proteins and NDH-1 in *Synechocystis* sp. PCC 6803. *The Plant Journal*, **103**, 1460–1476. Available from: https://doi.org/10.1111/tpj.14812

Nikkanen, L., **Solymosi, D.**, **Jokel, M.** & **Allahverdiyeva, Y.** (2021) Regulatory electron transport pathways of photosynthesis in cyanobacteria and microalgae: recent advances and biotechnological prospects. *Physiologia Plantarum*, **173**, 514–525. Available from: https://doi.org/10.1111/ppl.13404

Nikkanen, L., **Vakal, S.**, **Santana-Sanchez, A.**, **Hubacek, M.**, **Wang, Y.**, **Boehm, M.** ***et al.*** (2023) Proton motive force dissipation drives flavodiiron proteins to the thylakoid membrane for ferredoxin-powered O_2 photoreduction. *bioRxiv*. Available from: https://doi.org/10.1101/2023.05.19.541409

Origin (2016). *OriginPro Version 2016*. Northampton, MA, USA: OriginLab Corporation.

Peltier, G., **Aro, E.-M.** & **Shikanai, T.** (2016) NDH-1 and NDH-2 plastoquinone reductases in oxygenic photosynthesis. *Annual Review of Plant Biology*, **67**, 55–80. Available from: https://doi.org/10.1146/annurev-arplant-043014-114752

Peltier, G., **Tolleter, D.**, **Billon, E.** & **Cournac, L.** (2010) Auxiliary electron transport pathways in chloroplasts of microalgae. *Photosynthesis Research*, **106**, 19–31. Available from: https://doi.org/10.1007/s11120-010-9575-3

R Core Team. (2020) *R: a language and environment for statistical computing*. Vienna, Austria: R Foundation for Statistical Computing.

Santana-Sanchez, A., **Solymosi, D.**, **Mustila, H.**, **Bersanini, L.**, **Aro, E.-M.** & **Allahverdiyeva, Y.** (2019) Flavodiiron proteins 1–to-4 function in versatile combinations in O_2 photoreduction in cyanobacteria. *eLife*, **8**, e45766. Available from: https://doi.org/10.7554/eLife.45766

Santos-Merino, M., **Torrado, A.**, **Davis, G.A.**, **Röttig, A.**, **Bibby, T.S.**, **Kramer, D.M.** ***et al.*** (2021) Improved photosynthetic capacity and photosystem I oxidation via heterologous metabolism engineering in cyanobacteria. *Proceedings of the National Academy of Sciences of the United States of America*, **118**, e2021523118. Available from: https://doi.org/10.1073/pnas.2021523118

Santos-Merino, M., **Yun, L.** & **Ducat, D.C.** (2023) Cyanobacteria as cell factories for the photosynthetic production of sucrose. *Frontiers in Microbiology*, **14**, 1126032. Available from: https://doi.org/10.3389/fmicb.2023.1126032

Schmermund, L., **Jurkaš, V.**, **Özgen, F.F.**, **Barone, G.D.**, **Büchsenschütz, H.C.**, **Winkler, C.K.** ***et al.*** (2019) Photo-biocatalysis: biotransformations in the presence of light. *ACS Catalysis*, **9**, 4115–4144. Available from: https://doi.org/10.1021/acscatal.9b00656

Sétif, P., **Boussac, A.** & **Krieger-Liszkay, A.** (2019) Near-infrared in vitro measurements of photosystem I cofactors and electron-transfer partners with a recently developed spectrophotometer. *Photosynthesis Research*, **142**, 307–319. Available from: https://doi.org/10.1007/s11120-019-00665-2

Sétif, P., **Shimakawa, G.**, **Krieger-Liszkay, A.** & **Miyake, C.** (2020) Identification of the electron donor to flavodiiron proteins in *Synechocystis* sp. PCC 6803 by in vivo spectroscopy. *Biochimica et Biophysica Acta (BBA) - Bioenergetics*, **1861**, 148256. Available from: https://doi.org/10.1016/j.bbabio.2020.148256

Spasic, J., **Oliveira, P.**, **Pacheco, C.**, **Kourist, R.** & **Tamagnini, P.** (2022) Engineering cyanobacterial chassis for improved electron supply toward a heterologous ene-reductase. *Journal of Biotechnology*, **360**, 152–159. Available from: https://doi.org/10.1016/j.jbiotec.2022.11.005

Tan, C., **Xu, P.** & **Tao, F.** (2022) Carbon-negative synthetic biology: challenges and emerging trends of cyanobacterial technology. *Trends in Biotechnology*, **40**, 1488–1502. Available from: https://doi.org/10.1016/j.tibtech.2022.09.012

Theune, M.L., **Hildebrandt, S.**, **Steffen-Heins, A.**, **Bilger, W.**, **Gutekunst, K.** & **Appel, J.** (2021) In-vivo quantification of electron flow through photosystem I – cyclic electron transport makes up about 35% in a cyanobacterium. *Biochimica et Biophysica Acta (BBA) - Bioenergetics*, **1862**, 148353. Available from: https://doi.org/10.1016/j.bbabio.2020.148353

Torrado, A., **Connabeer, H.M.**, **Röttig, A.**, **Pratt, N.**, **Baylay, A.J.**, **Terry, M.J.** ***et al.*** (2022) Directing cyanobacterial photosynthesis in a cytochrome c oxidase mutant using a heterologous electron sink. *Plant Physiology*, **189**, 2554–2566. Available from: https://doi.org/10.1093/plphys/kiac203

Tüllinghoff, A., **Uhl, M.B.**, **Nintzel, F.E.H.**, **Schmid, A.**, **Bühler, B.** & **Toepel, J.** (2022) Maximizing photosynthesis-driven Baeyer–Villiger oxidation efficiency in recombinant *Synechocystis* sp. PCC6803. *Frontiers in Catalysis*, **1**, 780474. Available from: https://doi.org/10.3389/fctls.2021.780474

Van Thor, J.J. (1999) Localization and function of ferredoxin:NADP+ reductase bound to the phycobilisomes of *Synechocystis*. *The EMBO Journal*, **18**, 4128–4136. Available from: https://doi.org/10.1093/emboj/18.15.4128

Viola, S., **Sellés, J.**, **Bailleul, B.**, **Joliot, P.** & **Wollman, F.-A.** (2021) In vivo electron donation from plastocyanin and cytochrome c6 to PSI in *Synechocystis* sp. PCC6803. *Biochimica et Biophysica Acta (BBA) - Bioenergetics*, **1862**, 148449. Available from: https://doi.org/10.1016/j.bbabio.2021.148449

Wang, Y., **Chen, X.**, **Spengler, K.**, **Terberger, K.**, **Boehm, M.**, **Appel, J.** ***et al.*** (2022) Pyruvate:ferredoxin oxidoreductase and low abundant ferredoxins support aerobic photomixotrophic growth in cyanobacteria. *eLife*, **11**, e71339. Available from: https://doi.org/10.7554/eLife.71339

Wey, L.T., **Bombelli, P.**, **Chen, X.**, **Lawrence, J.M.**, **Rabideau, C.M.**, **Rowden, S.J.L.** ***et al.*** (2019) The development of biophotovoltaic systems for power generation and biological analysis. *ChemElectroChem*, **6**, 5375–5386. Available from: https://doi.org/10.1002/celc.201900997

Wlodarczyk, A., **Gnanasekaran, T.**, **Nielsen, A.Z.**, **Zulu, N.N.**, **Mellor, S.B.**, **Luckner, M.** ***et al.*** (2016) Metabolic engineering of light-driven cytochrome P450 dependent pathways into *Synechocystis* sp. PCC 6803. *Metabolic Engineering*, **33**, 1–11. Available from: https://doi.org/10.1016/j.ymben.2015.10.009

Yadav, R.M., **Aslam, S.M.**, **Madireddi, S.K.**, **Chouhan, N.** & **Subramanyam, R.** (2020) Role of cyclic electron transport mutations pgrl1 and pgr5 in acclimation process to high light in *Chlamydomonas reinhardtii*. *Photosynthesis Research*, **146**, 247–258. Available from: https://doi.org/10.1007/s11120-020-00751-w

Zhang, P., **Allahverdiyeva, Y.**, **Eisenhut, M.** & **Aro, E.-M.** (2009) Flavodiiron proteins in oxygenic photosynthetic organisms: photoprotection of photosystem II by Flv2 and Flv4 in *Synechocystis* sp. PCC 6803. *PLoS One*, **4**, e5331. Available from: https://doi.org/10.1371/journal.pone.0005331

Zhang, P., **Eisenhut, M.**, **Brandt, A.-M.**, **Carmel, D.**, **Silén, H.M.**, **Vass, I.** ***et al.*** (2012) Operon *flv4-flv2* provides cyanobacterial photosystem II with flexibility of electron transfer. *Plant Cell*, **24**, 1952–1971. Available from: https://doi.org/10.1105/tpc.111.094417